communications earth & environment

Article

https://doi.org/10.1038/s43247-024-01709-9

Carbonate mud production in lakes is driven by degradation of microbial substances

P. Boussagol[1], **E. Vennin**[1] ✉, **F. Monna**[2], **L. Millet**[3], **A. Bonnotte**[4], **S. Motreuil**[1], **I. Bundeleva**[1], **D. Rius**[3] & **P. T. Visscher**[5]

Carbonate mud is crucial in the global carbon cycle and serves as a key sedimentary archive for paleoclimate reconstruction. Understanding the mechanisms behind its formation is crucial for explaining long-term carbon storage, including atmospheric carbon dioxide transfer to the hydrosphere and variations in mud production over geological timescales. Various mechanisms explain carbonate mud formation in both lake and marine sediments. Using bio-physicochemical methods on deep sediments of Lake Ilay, Jura, France, we propose a model of micrite formation. Our study shows that micrite mineralization occurs in sediments due to the degradation of ooze rich in exopolymeric substances throughout the sediment core's depth. This mineralization continues as long as exopolymeric substances are present, persisting for at least 2000 years. Cryo-Scanning electron microscope imaging reveals calcite nucleation at degraded exopolymeric substance nodes, advancing with substance degradation and calcium release. These findings provide insights into fossil carbonate mud origins and formation processes.

Carbonate mud represents a major reservoir in the global carbon cycle[1] and one of the main sedimentary archives for reconstructing climate[2,3]. Despite these important roles, the origin of carbonate mud (particle diameter <62.5 µm) in lacustrine and marine environments is a yet unresolved sedimentary conundrum. A better understanding of the mechanisms involved in carbonate mud formation is therefore critical to explain the sedimentary carbon storage, including the CO_2 transfer from the atmosphere to the hydrosphere and variations in mud production that are observed over geological timescales[4]. The significance of carbonate mud formation is further underscored by the massive annual atmospheric carbon burial in modern lakes, associated with increasing atmospheric CO_2 boosted by anthropogenic activity since the start of the industrial revolution[5]. Estimates indicate that lacustrine sinks represent about one fifth of the marine carbon burial[5,6]. Several mechanisms are proposed to explain the formation of carbonate mud in the sediments of both lakes and marine systems. The most commonly accepted models suggest a precipitation of crystals in the water column[1] related to: (1) degradation of calcareous green algae[7,8]; (2) precipitation during "whiting events"[9–11] and (3) biologically-induced by the degradation of microbial extracellular polymeric substances (EPS), which releases Ca^{2+} and CO_3^{2-}[12]. These processes form fine-grained carbonate particles that ultimately sink to the sediment[10,13]. These sediments are mixed with intraclasts, picoplankton calcite tests and skeletal grains at the water/sediment interface ultimately forming the carbonate mud[4,14]. In addition, precipitation of calcite crystals can occur in EPS produced at the microbial mats surface[15–17]. EPS are excreted by cyanobacteria[18,19] and other mat inhabitants[20] and make the microbial mat gelatinous and sticky. These EPS consist of polysaccharides, proteins, with small amounts of extracellular DNA, exoenzymes, trace metals, and minerals. Carbonate precipitation mediated by microbial processes have been suggested in discreet layers[21,22] but, to date, actual mechanisms along the depth of the sediment column have not been resolved.

To fill this gap in our knowledge, this study aims to identify the process of formation of micrite (<4 µm), the main constituent of the carbonate mud in lakes. To accomplish this, we investigated a 1.2 m-long core representing the most recently deposited sediment in the lake at 8.4 m water depth (Supplementary Fig. 1). The upper 1.2 m were sampled and prepared for Cryo-SEM analysis as well as EPS quantification and microbial degradation potential.

In this study, we demonstrated unequivocally that carbonate precipitation was sustained at depth in sediments of Lake Ilay (Jura, France;

---

[1]Biogéosciences, UMR 6282 CNRS, Université de Bourgogne, Dijon, France. [2]ARTEHIS, UMR 6298 CNRS, Université de Bourgogne, Dijon, France. [3]Laboratoire Chrono-Environnement, UMR6249 CNRS, Université de Franche-Comté, Besançon, France. [4]Plateforme DImaCell, Agroécologie, INRAE, Institut Agro, Université de Bourgogne, Dijon, France. [5]Departments of Marine Sciences & Earth Sciences, University of Connecticut, Storrs, CT, USA.
✉e-mail: Emmanuelle.vennin@u-bourgogne.fr

Fig. 1 and Supplementary Note). The micrite mineralization occurred predominantly in the sediment, not in the water column, and resulted from EPS degradation along the entire depth of the sediment core (Fig. 1). As long as there is organic matter to degrade, even at the bottom of the core which covers at least two millennia; (Fig. 1), active carbonate mud production continued. A conceptual model depicting the role of EPS in carbonate production (formation in the water column and/or water-sediment interface and degradation in the sedimentary column) is proposed in Fig. 2a.

Results and discussion

Sedimentary column

The 120 cm-long core comprised alternating organic-rich layers and carbonate mud (micrite and biogenic remains). The upper 20 cm consisted of microbial "ooze", with a green coloration and a lumpy, gelatinous texture. With depth, gelatinous layers diminished and micritic microbial-rich muddy sediment increased, which was illustrated by alternating lighter (Total Organic Carbone, TOC, mean content: 4.6%; Supplementary Table 1) and darker layers (TOC, mean content: 12.1%), respectively. From the activity profile of the short-lived artificial ^{137}Cs radionuclide, two sedimentary layers can be precisely dated (Supplementary Fig. 2). The first peak, which appears at a depth of 14.5 cm, corresponds to the fallout of cesium following the Chernobyl accident in 1986[23]. The second peak, located at a depth of 37.5 cm, which is also the largest, is recognized worldwide and estimated to have occurred in 1963/64[24,25], consequently to the signing of the Partial Test Ban Treaty in August 1963, which banished nuclear weapon tests in the atmosphere. Moreover, the first appearance of ^{137}Cs in the sedimentary column at a depth of 50 cm also provides an interesting dating constraint. Although inputs of artificial ^{137}Cs began to contaminate the global environment around 1952[25], it is generally accepted that the first detectable ^{137}Cs fallout, ubiquitous around the world, corresponds to the 1954–1955 period[24]. On the other hand, a ^{14}C analysis obtained from a leaf sampled just one centimeter below (i.e., 51 cm depth) yielded a radiocarbon age of 210 ± 30 BP which belongs, once calibrated and expressed in calendar dates, to the [1642-present cal. AD] time interval (See "Method" section). Given the time control provided by the aforementioned first ^{137}Cs detection, it is reasonable to assume that this sedimentary layer was deposited around the late 40 s to early 50 s. Two other organic samples collected at depths of 80/81 cm and 110/111 cm provided radiocarbon ages at 1810 ± 30 BP and 2150 ± 30 BP, respectively. Details and calibrations can be found in the "Method" section and in Supplementary Material. However, since the primary aim was not to determine the sedimentation rate or other kinetics with high precision but rather to give a general overview of the time span covered by the core, these two samples were simply assigned to the 2nd-4th centuries AD and the 4th-1st centuries BC, respectively. This clearly indicates that our core spans at least the last two millennia.

X-ray diffraction analyses of the mineralogical fraction revealed predominantly calcite over the entire depth of the core. Furthermore, the dry density showed an increasing trend below the first 57 cm, but with a slight fluctuation of $CaCO_3$ (78% ± 6) and water content (75.4% ± 2.36). This suggested that the volumic concentration of calcite increased with depth, which was confirmed by Cryo-SEM observations, minimizing the influence of compaction (Fig. 1 and Supplementary Table 1). From a depth of 57 cm to the bottom of the core, we found a more variable calcimetry and density that could be explained by a variable organic matter content. A major change of the C:N ratio was noted at 44 cm. From the top down to a depth of 44 cm, the C:N ratio slightly increased from 8 to 11.5, such value indicating organic matter of algal or microbial origin[26]. This increase could result from the selective consumption of N-containing molecules in EPS by microbes[27] but can also be explained by the presence of remnants of terrestrial plants (Supplementary Fig. 3 and Table 1). Between 44 and 80 cm, the C:N ratio increased from 12.5 to 15. Between 80 and 100 cm, the ratio decreased from 14 to 10 and downcore, the ratio evolved from 11 to 14. The abundance and size (ranging from 0.5 μm to >10 μm) of calcite crystals in the sediment increased progressively with depth.

Exopolymeric ooze

An EPS-rich ooze on the top of the core was observed when the water depth of the lake exceeded 5 m (Fig. 1; Supplementary Fig. 4). This microbial ooze had no defined boundary with the underlying sediment and ranged from 1 to 20 cm in thickness (Supplementary Fig. 4b–d). This ooze transitioned laterally to a cohesive mat in the shallow part of the lake (where the water depth was less than ~5 m; Supplementary Fig. 5a to f). The ooze displayed only minor mineralization but evolved into microbial carbonate mud with depth in the core (Supplementary Fig. 4e–g). The ooze, with a high EPS content, had a similar biological composition with diatoms and filamentous bacteria, as the mat that was found at a shallower water depth. Downcore cryo-SEM observations of microbial carbonate mud confirmed that EPS were preserved along the entire sedimentary column with an increasing degree of alteration with depth (Fig. 1). The degradation of the EPS is corroborated by the typical shape of a polygonal matrix[28] that resembled a spider web, increasingly airier with depth (Fig. 1). The EPS content decreased from the top to the bottom of the sedimentary column, particularly in the first 50 cm. In the upper ~30 cm of the core, acidic functional groups (with a strong binding capacity for cations such as calcium), proteins, and structural sugars in EPS all declined by approximately one order of magnitude (Fig. 1d). The ratio of both protein to acidic groups remained constant in this depth interval, but ratio of sugar to acidic groups varied, indicative of a major contribution of the protein fraction in calcium binding. However, the sugar to protein ratio increased sharply with depth, suggesting an expected preferential removal of the protein fraction by heterotrophic microbial decay[27]. EPS-degrading microbial enrichments were readily obtained from various depths of the core. Three layers at depth of 12, 44–47, and 112 cm were sampled and enriched (mat and met). These layers were incubated with 2 g . L^{-1}dextran-sulfate (a model EPS) as the sole source of carbon. Under these conditions, heterotrophic microbial activity consumed 71, 49, and 58 % of those EPS, respectively, over a 10-day period. The remaining EPS presumably represents a highly recalcitrant fraction[29]. Degradation at the top occurred in the presence of oxygen and was thus likely more rapid than at depth, where anaerobic respiration prevailed. It is well known that aerobic respiration, which needs more energy, typically outpaces anaerobic respiration, in particular in the case of complex polymer (i.e., EPS) degradation[30,31].

Crystal morphology

Cryo-SEM revealed four different carbonate crystal morphologies (Fig. 2b): (i) polyhedral (Supplementary Figs. 6, 7a, b), (ii) pyramidal (Supplementary Fig. 8a), (iii) sub-spherical (Supplementary Fig. 8b) (iv) and bladed (Supplementary Fig. 8c, d). The largely dominating polyhedral crystals were composed by rhomb-shaped crystallites (Supplementary Fig. 7c–h). The polyhedral crystals appeared in the first few centimeters of the sedimentary core as isolated crystals (1 to 2 μm). With increasing depth, these crystals grew in size (up to 10 μm) and abundance, ultimately forming clusters that filled the residual porosity (Fig. 1 and Supplementary Figs. 6, 7, and 9). Pyramidal crystals were only observed deeper in the core and were less common than polyhedral crystals. These pyramidal crystals comprised an agglomeration of rhomb-shaped crystallites up to 2 μm in size. Bladed crystals were rare and consisted of tightly packed needle crystallites (Supplementary Fig. 8d–g). The sub-spherical crystals were composed of a combination of needle and rhombic crystallites (Fig. 2b). Both the needle and rhombic crystallites resulted from the clustering of nano-globules (<50 nm; Supplementary Figs. 6a, b, and 8h).

Regardless of morphology and growth stage, all crystals were consistently embedded within the EPS matrix and nucleated mainly at the polygon nodes (Supplementary Figs. 6a–f, 7, and 8). This strongly indicated that crystal growth occurred during EPS degradation. The presence of nano-globules on the surface of the crystals indicated that this growth continued with depth in the sediment column until all the EPS were completely degraded[32] (Supplementary Fig. 8h). With increasing depth, carbonate minerals showed clearer crests, which was particularly evident in the polyhedral morphologies. Ultimately, this resulted in a filled crystal with

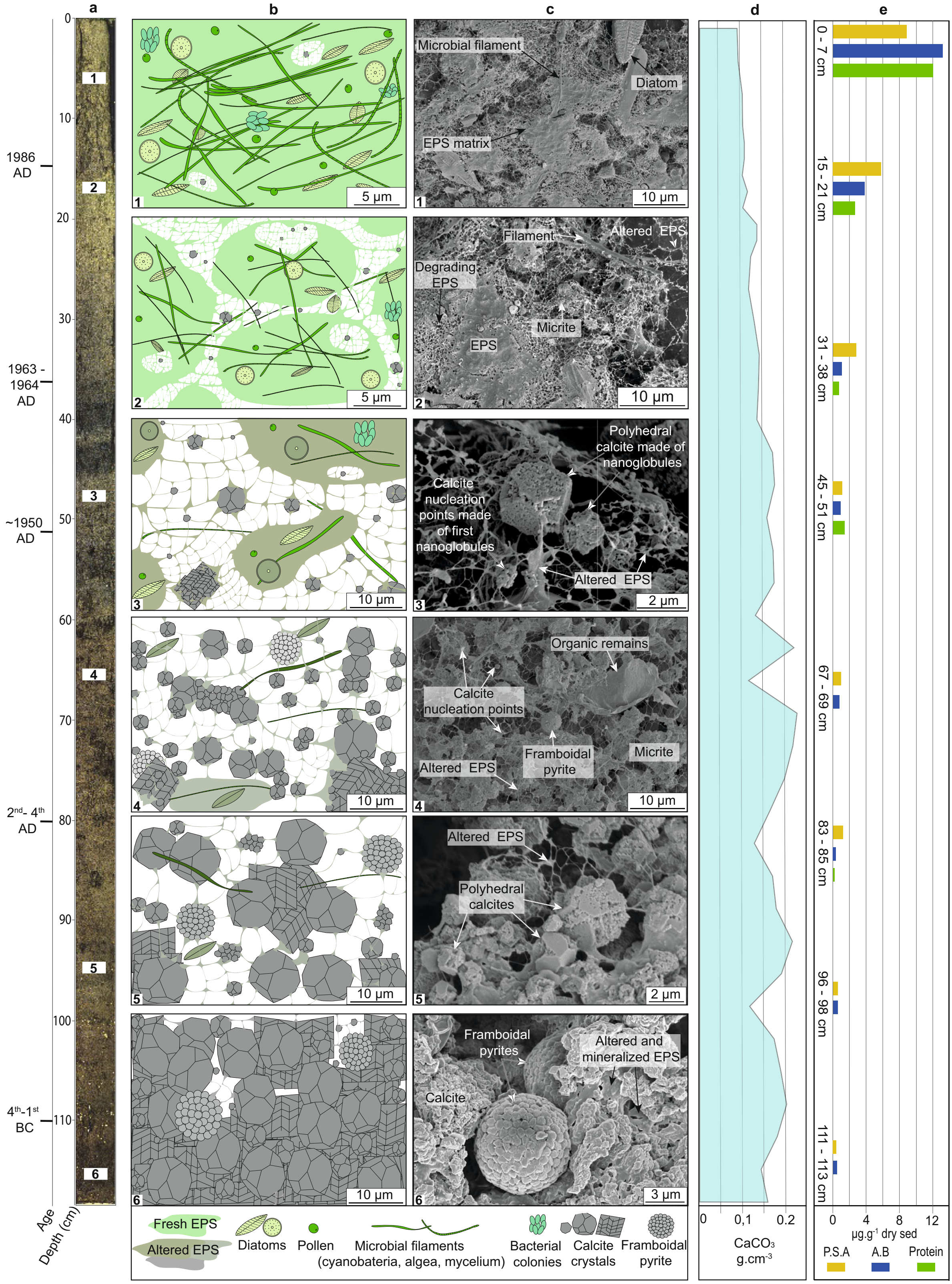

Fig. 1 | Dataset of the Lake Ilay sediments, Jura (see Supplementary Note and location map-Supplementary Fig. 1). a 1.2 m-long core section showing the position of the samples shown in (**b**, **c**, **e**) (1–6). **b** Cartoons showing an increase in calcite crystal with depth based on cryo-scanning electron microscopy (Cryo-SEM) observations. **c** Cryo-SEM images of the samples from top to the bottom of the core section (scale bar is 10 µm) with (from top to bottom in panel): **1** Microbial communities (filaments in EPS, diatoms, and organic components). **2** Matrix with degrading EPS with a characteristic honeycomb structure and micritic precipitate. **3** Polyhedral calcite crystal composed of nano-globules embedded in altered (i.e., partially degraded) EPS. **4** Calcite crystals embedded in altered EPS, with organic remains and framboidal pyrites; calcite nucleation points are observed at the node of EPS structures. **5** Polyhedral calcite crystals with perfect rhombic unfilled faces embedded in altered EPS. **6** Rich-calcite micrite matrix with framboidal pyrites. **d** Calcium carbonate calcimetry with depth (gr.cm^{-3}). **e** Major EPS constituents (µg . g^{-1} dry sediment): proteins, acidic groups (Alcian Blue; A.B), and structural sugars (phenol-sulfuric acid assay; PSA).

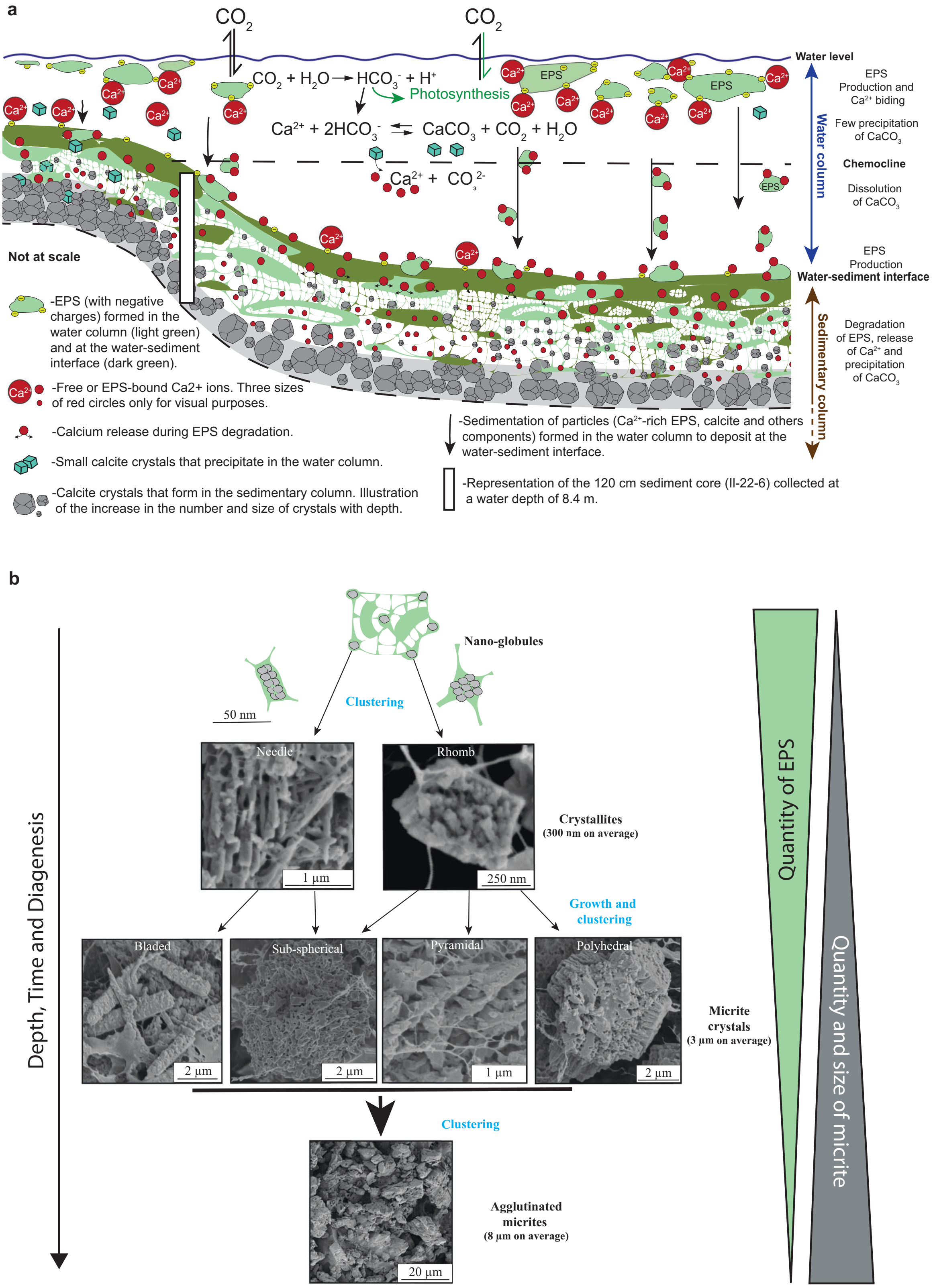

Fig. 2 | Modeled temporal evolution of the crystal calcite. a Conceptual model illustrating the process of Ca^{2+} and HCO_3^- capture and release in Lake Ilay. It shows the exchange of CO_2 between the atmosphere and the lake, the metabolism of CO_2 and HCO_3^- by photosynthesis, capture of calcium in EPS in the water column, and at the sediment-water interface, and the release of calcium in the sediment when EPS degraded conducing to carbonate precipitation. **b** Development showing an evolution from nano-globules (less than 50 nm), clustered in needle and rhomb crystallites (300 nm in average), then organized during their growth in micrites: bladed, sub-spherical, pyramidal and polyhedral crystals (3 µm in average) building the agglutinated micrites (mean of 8 µm). The formation of micrite (size and quantity) is associated with an increase in EPS degradation and decrease in EPS quantity.

perfect planar rhombic faces, which contrasted the unfilled faces observed in the uppermost centimeters of the core. The crystal faces developed through a progressive occlusion of the remaining EPS-filled cavities (Fig. 1). Thus, we established that micrite crystal growth was achieved by successive addition of crystallites, that in turn were made through progressive addition of calcite nano-globules (Fig. 2b; Supplementary Fig. 7c–e).

EPS role in binding and releasing of calcium

The sequential replacement observed of EPS by calcium carbonate was active down to at least 1.2 m, i.e., the bottom of our core. Microbial activity at several meters depth has been documented in a variety of environments[33,34], and can be supported by aerobic and anaerobic heterotrophic bacterial activity degrading EPS[16,20,35,36]. EPS degradation has been linked to carbonate precipitation, notably in microbial mats[12,37,38]. Initially, EPS act as inhibitors of carbonate precipitation by limiting access to nucleation sites due to its 3D architecture. The consecutive degradation of EPS leads to the creation of space around the nucleation points and encourages crystal growth[39].

EPS are produced by a variety of organisms in the water column, such as phototrophic organisms, like cyanobacteria[40], diatoms[41] and heterotrophic bacteria[40]. However, the difference in EPS properties between the water column and sediments in Lake Ilay suggests an important production by the benthic microbial community at the water/sediment interface. Thus, the EPS in the ooze do not result solely from the settling from the water column (Supplementary Table 2). Although we cannot rule out that the difference in polymer composition is due to degradation of water column EPS, the large amount of ooze with different properties at the sediment surface implies a major role for benthic production of EPS. Irrespective of changes in composition between water column and sediments, the abundance of acidic groups in protein of EPS at the sediment interface represented a major calcium binding potential. The negatively-charged functional groups in fresh EPS bind free cations (such as Ca^{2+}) directly from the surrounding solution[12], initially inhibiting $CaCO_3$ precipitation[12,40]. Upon saturation of the binding sites, microbial degradation of the EPS releases Ca^{2+} and HCO_3^- allowing $CaCO_3$ to nucleate on the organic matrix[12,28,38]. As demonstrated in previous studies[29,42] and here, various heterotrophic bacteria consume EPS as a carbon source through enzymatic degradation.

Calcium budget in a lake system

In our study, we found a high binding capacity of the calcium to EPS at the water/sediment interface, which was also documented in the water column[43] (Supplementary Table 2). The calcite saturation indices, based on free calcium, fluctuated between 0.56 and 0.87 in the water column (Supplementary Table 3), and thus the pelagic mineralization capacity is reduced or inhibited depending on the season. EPS analyses carried out in May 2023 in the water column showed that the calcium bound to this polymer matrix can be up to four times greater than the amount of free calcium ($47.2\,mg\,.\,L^{-1}$ [43]). It should be noted that we cannot discard the occasional whiting events that could deliver $CaCO_3$ particles in water column[11], but these have not been observed in Lake Ilay in the frame of this study.

We recorded a progressive decrease in EPS preservation downcore and an increase in free Ca^{2+} in the pore water ($93.23\,mg\,.\,L^{-1}$; Supplementary Table 4). Thus, we can assume that the degradation of these polymers released calcium ions. This would locally increase the saturation index to >0.9 and consequently, the mineralizing capacity (Supplementary Table 4), allowing the precipitation of calcite in the sediment[15,21,28,29,32,44]. This is further corroborated by the decrease of EPS with depth and the presence of heterotrophic microbial polymer degrading enrichment cultures, that could be obtained from different depths throughout the core. Furthermore, the negative charged groups in the water column EPS and that in the ooze at the sediment surface trap Ca^{2+}, making it unavailable for calcite precipitation. This provide a source of calcium deeper in the sediment when the protein/acidic groups decrease rapidly, and local nucleation commences as less Ca^{2+} is bound. In this scenario, carbon is predominantly supplied through the degradation of EPS and organic matter present in pore water.

Carbonate production in the sedimentary column

During burial, the subsurface sediment undergoes early diagenetic alteration through microbial and physicochemical processes. Based on the progressive EPS degradation and increasing calcite content with depth in our core, we postulate that the micritic mineralization takes place over a prolonged period (at least two millennia) supported by the degradation of the EPS downcore. The continuous presence of EPS surrounding sediment particles with an increasing degree of alteration and the abundance of biological remnants (e.g., filaments, diatoms or pollen) suggest that these sediments are formed from degrading microbial ooze. Thick filamentous sheaths that are part of the ooze could represent remnants of cyanobacteria preserved during early diagenesis[45]. They are typically present in deeper layers of microbial mats[28]. The production of carbonate minerals within the sedimentary column rather than in the overlying water fueled by benthic EPS degradation, therefore, requires that the microbial ooze has sufficient calcium storage capacity to sustain active $CaCO_3$ precipitation, even after millennia of burial.

Nucleation points and crystal growth

Nucleation points, defined as nano-globules forming mineral clusters, were observed at the junction between several EPS structural polygons (i.e., the nodes in the honeycomb structure; Supplementary Fig. 9) as proposed by Dupraz et al. [28] and Luo et al. [32]. No nanobacteria or viruses were observed in the vicinity of these polygons. These clusters were observed throughout the entire depth of the core, with an increasing abundance in the layers where EPS degradation was more pronounced (Fig. 1; Supplementary Fig. 6a, b). The clustering of nano-globules results in the formation of small crystallites (around 500 nm) with rhomb and needle shapes[46]. Overgrowing of these crystallites forms calcite crystals constituting micrite (Fig. 2b). SEM observations showed the progressive growth of crystal faces and edges towards regular geometric shapes with depth. Consequently, the crystal growth is progressive with burial due to combined physicochemical and microbial activity (EPS degradation). Despite the crystals are angular in shape, they are not necessarily the result of abiotic processes, contrary to what is often proposed in the literature[47].

These observations imply that the crystallization of carbonate minerals takes place in metabolically active sediments until the EPS matrix is completely depleted. When considering the association of micritic crystals and framboidal pyrite embedded in the EPS matrix, a similar mechanism of nucleation and growth can be invoked (Supplementary Fig. 10).

EPS were present to the bottom of a 1.2 m-lake sediment core, but the properties changed with depth. Notably, the amount and relative abundance of negatively charged, cation-binding functional groups decreased with depth. Fresh EPS initially scavenged calcium ions, thus initially limiting the carbonate precipitation. Consecutive microbial heterotrophic degradation of EPS deeper in the core released calcium and produced inorganic carbon. This locally increased the saturation index and actively promoted calcite precipitation, even at bottom of the core. Although the composition of the EPS in the water column and at the water/sediment interface differed (Supplementary Table 2), both contribute to calcium storage. Calcium is thus initially a limiting reactant for the carbonate precipitation. Our dating confirms that sediments as old as the beginning of our era remain the locus of microbial carbonate precipitation. This was further supported by cryo-SEM images of degraded EPS showing nucleation and the growth of calcite crystals at the bottom of the core. Calcite nucleation points are observed at the nodes of degrading EPS polygons and increase with depth in association with advanced stages of EPS degradation. These nucleation points include calcite nano-globules that agglomerate to form crystallites, the growth and accretion of which lead to the formation of crystals of calcite. Down the core section, we show an increase in the size of the well-shaped crystals with filled faces and clear crests.

The formation of micrite in sediments during burial raises questions about the origin of carbonate microcrystalline minerals preserved in the fossil record. Importantly, the conservation of their isotopic signals and offers a novel insight into their formation. Carbonate production in Lake

Ilay is positively influenced by factors linked to increased atmospheric CO_2 concentrations, including increased alkalinity and intensified photosynthesis by EPS-producing phototrophs like diatoms and cyanobacteria[48]. The resulting production of EPS in the water column increases calcium trapping, transporting this to the sediments following settling from water column. In Lake Ilay, most of the carbonate production thus occurs progressively through sedimentation and the degradation of these EPS, releasing Ca^{2+} in the sedimentary column (Fig. 2a). The carbonate precipitation, during early diagenesis, leads to the long-term sequestration of carbon, whereas in contrast, modern accumulation of organic matter is a short-term sequestration. This major role of CO_2 storage as carbonate contemporary mud needs further consideration.

Online methods

Terminology

The terminology for crystal size and shape is from Folk[49]. Rhombic refers to euhedral rhombohedral crystals with 6 rhombuses, whereas polyhedral refers to multi-faceted crystals having more than 6 faces. The terms euhedral, subhedral, and anhedral refer to crystals with well-defined, moderately defined, and poorly defined crystal faces, respectively[50]. As calcite morphogenesis is not beyond the purpose of this manuscript, we consider that the different morphology may result from the complex interaction between different physico-chemical parameters which often act simultaneously (e.g., carbonate mineral supersaturation, Mg/Ca ratio of the parental fluid, organic and inorganic additives). Mercedes-Martin et al. [51] discuss the driving forces at the origin of calcite morphogenesis and considered two competing mode of calcite precipitation: the calcite supersaturation level of the parental fluid, and the concentration of microbial-derived organic molecules (alginic acid).

The term micrite is here used as proposed by Folk[52] and as a compound-acronym for “microcrystalline calcite”. The term micrite is used to address fine-grained carbonate that is, for the most part, smaller than 4 µm in size, independent of the calcite or aragonite mineralogy[53,54].

Field sampling

Sediment core sampling. All sedimentological analyses and observations were based on a sediment core collected on 11/24/2022 on the western shore of lake Ilay (Lat 46.625640°, Long 5.895115°) at a water depth of 8.4 m. The 1.2 m sediment core was retrieved using an Uwitec gravity corer fitted with a 63 mm diameter PVC tube. In the laboratory, the sediment core was split into two equal halve and stored under UBGD.300450 (Biogeosciences-Recolnat). Sediment samples were stored in the dark at 4 °C until processing.

Lake water sampling and in situ analysis. To monitor variations in the physiochemical conditions of the water column of Lake Ilay, a multiparameter probe (In Situ, Aqua TROLL® 500, Fort Collins, USA) was installed on 05/11/2022 to measure continuously (every 6 h) pH, the electrical conductivity, the chlorophyll a concentration, turbidity and temperature of the lake water. The probes were supported by a buoy at a depth of 2 m and connected to a modem using the HydroVu (In Situ, Fort Collins, USA) software for database storage. This monitoring was supplemented by water sampling and by field measurements (see details in Supplementary Table 3) of pH and electrical conductivity with portable pH/Cond multi-parameter probe (ProfiLine® 3320 WTW®, Weilheim, Germany). The spot measurements covered the entire lake at different periods of the year. Depth-dependent measurements are also taken using a 2 L Niskin bottle/Water Sampler (Bionef® Ruttner Standard Water Sampler, Montreuil, France). The water samples collected were processed using a 0.22 or 0.45 µm-membrane filter and are stored cold before analysis.

Analysis of water chemistry

Concentration of major ions were measured using the ion chromatography method with a Dionex® DX100 (Thermo Fisher Scientific, Waltham, MA, USA) installed at Biogéosciences laboratory (Dijon, France), whereas Ca^{2+} concentrations were obtained by flame atomic absorption spectroscopy (AAS), using a AAnalyst 400 (PerkinElmer Instruments, Wellesley, MA, USA). For both methods, homemade solutions of known concentrations were inserted in the sample list to check data accuracy. For ion chromatography, uncertainty and detection limit can be estimated to be 3×10^{-5}M while for AAS this parameters are lower than 2% and 2 µg . L^{-1}, respectively. The Gran titration method[55] using 0.01 N solution of HCl in laboratory was used to assess the total alkalinity. The flame atomic absorption spectroscopy and Gran Titration analyses were carried out at the Geosciences Environment Toulouse laboratory (GET, Toulouse, France). The saturation index (SI) values of calcite and aragonite was calculated in all water samples by using software PHREEQC Interactive (version 3.6.2) and the respective database[56,57]. The values of pH, alkalinity, temperature, and calcium concentration measured at the time of sampling were used for these calculations. Generally, the calcite saturation index corresponds to the threshold above which calcite precipitates. (Super)saturation conditions are given when $SI_{calcite} \geq 0$, but spontaneous calcite precipitation apparently needs a supersaturation of at least SI = 0.8[58]. The SI values measured in the surface waters of Lake Ilay are presented in Supplementary Table 3, combined with the pH, conductivity, and Ca^{2+} concentration values.

To determine the physico-chemical properties of the pore-water contained in the carbonate sludge of Lake Ilay, four other sediments cores were collected in the immediate vicinity of the main core. To be as close as possible to the area of interest, the cores were extracted by divers using plexiglass tubes. The same day, the cores are pierced, and the pore water collected using a Rhizon system. Two to four water micro samplers were connected per core. All sampling systems are activated at the same time on the same core to minimize water migration within the cores. Only one sample was collected in sufficient quantity for analysis of elemental composition and alkalinity. The other samples were analyzed with a multiparameter probe for pH and conductivity, as explained previously. Results are presented in supplementary Table 4.

Dating

Three radiocarbon ages were obtained from terrestrial material. After sieving the sediment at 200 µm, the terrestrial macro vegetal remains were carefully sorted using fine forceps under a stereo-microscope at 10–60 X magnification. Between 20 mg and 100 mg of material were extracted at three depths: 51 cm (leaves), 80–81 cm (charred leaves), and 110–111 cm (wood). Radiocarbon dating was performed at the Beta Analytic Laboratory (Miami, Florida) using Accelerator Mass Spectrometry (AMS), after applying a standard pretreatment protocol. The samples were first gently crushed, dispersed in deionized water, washed with hot HCl acid to eliminate carbonates, and then with NaOH to remove secondary organic acids. The final step consisted in an acid rinse to neutralize the solution before drying.

The three radiocarbon ages were calibrated using the OxCal software (v.4.4) using the IntCal20 calibration curve[59,60], providing calibrated calendar dates with their 95% confidence intervals (see Supplementary Methods).

Concerning the ^{137}Cs measurement, samples were extracted from bulk mud along from the top deep to 50 cm. They were dried at 60 °C during 48 h and crushed. A known mass of sediment was then filled in petri dishes. Activity of the short-lived radionuclide ^{137}Cs were measured each 2 cm up to 50 cm depth using a gamma spectrometer (Canberra Spectrometer- GeHP® detector, CO, USA), installed at the Chrono-Environment Laboratory. The artificial ^{137}Cs radioisotope emits at 661 keV. The spectra were deconvoluted and the extremely small background that may still exist at 661 keV was not taken into account in the calculation of ^{137}Cs mass activity. The spectrometer was calibrated with a standard of known radioactivity supplied by the IAEA to ensure the reliability of measurements.

Cryo-SEM observations

Fresh samples were collected directly from the cored section every time there is a change in facies (carbonate and organic matter estimation), texture (slime and granular) or color (dark brown to green creme layers) and prepared for Cryo-SEM analysis. This method of analysis, mainly used in biology, does not denature the samples, unlike traditional SEM methods. The sediments were not dehydrated or dried, but directly cryogenically frozen and only metallized with platinum to increase the conductance. The mud (i.e., ooze) surface was characterized by cryo-scanning electron microscopy (cryo-SEM) using a high-resolution field emission scanning electron microscope (FE-SEM, SU 8230, Hitachi High-Technologies, Tokyo, Japan) equipped with a cryo-preparation unit (Quorum PP3010T). Prior to imaging, samples were cryofixed into the pasty nitrogen slusher pot of the workstation, and cryofixed samples were transferred to the cryo-stage (PP3010T, Quorum, Laughton, UK). Following, they were sublimated at −90 °C for 10 min and coated with a thin platinum layer by sputtering at 10 mA for 15 s.

EPS extraction and analysis

EPS was extracted using 100 mM EDTA solution[42]. After centrifugation, and threefold precipitation in cold ethanol, followed by a second centrifugation step, the EPS content in each layer was measured with anionic functional groups using the Alcian Blue assay[61], reducing sugars using the phenol-sulfuric acid method[62], and protein. Xanthan and bovine serum albumin were used as standards[42,45].

Microbial enrichment and EPS degradation potential

Aliquots of sediment sampled at the depth of 12, 44–47, and 112 cm were transferred to sterile mineral media that contained 0.2 g . L^{-1} of NH_4Cl, 0.225 g . L^{-1} of $CaCl_2$-$2H_2O$, 0.2 g . $L^{-1}$of KCL 0.2 g . L^{-1} of $MgCl_2.6H_2O$, 0.02 g . L^{-1} of anhydrous KH_2PO_4, and 2.0 g . L^{-1} of anhydrous Na_2CO_3, supplemented with 0.1% yeast extract[63]. The medium was amended with mannose, fructose, gluconate, glutamate, aspartate, glutamine (50 mM final concentration each) and 0.1% dextran sulfate (Sigma Co, Missouri, St. Louis, USA). The inoculum from 12 cm depth was grown aerobically, the other samples were incubated anaerobically in medium purged with N_2. After two transfers to fresh medium, enrichments from each depth were transferred to a mineral medium with 1.0% dextran sulfate (a model EPS[40,45]) as the sole source of organic carbon and 0.05% yeast extract. Alcian Blue assays at the start and after 10 days of incubation at room temperature showed 71, 49, and 58% degradation in the enrichments obtained from 12, 44–47, and 112 cm depth, respectively.

Mineralogical analyses

The mineralogical composition of the mud samples was analyzed by X-ray diffractometry at the Biogéosciences laboratory (Dijon). Samples were ground in an agate mortar and analyzed using a Bruker D8 Endeavor diffractometer (Bruker Corporation, Billerica, MA, USA) with CuKα radiations combined with a LynxEye XE-T detector, under 40 kV voltage and 25 mA intensity. Elemental compositions of selected crystals were analyzed using an UltraDry EDS detector (Thermo Scientific, Waltham, MA USA) coupled to Cryo-SEM.

Dry bulk density, total organic carbon (TOC), Total nitrogen (TN)

Samples were collected every centimeter over the first thirty centimeters, then every two centimeters covering the entire core. The sediment samples were dried (60 °C, 48 h) until reaching constant weight, and water content (WC) was calculated from the weight loss. and powdered. Dry bulk density was determined from the weight of the dry sediment sample divided by the total sample volume. The ratio of wet to dry sediment weights allows us to estimate the water content of the entire cored sample, expressed in percent.

Total organic nitrogen and carbon concentrations (% dry mass) were contiguously measured from Lake Ilay core with a Vario-max CNS analyzer (Elementar) using 10–100 mg (according to the expected % Corg content to avoid saturation of the detector) of dried material from 2 cm-thick samples following the procedure described in ref. 64. A certified reference material of highly organic sediment (B2150), with known carbon and nitrogen concentrations ($C = 7.45\% \pm 0.14\%$ and $N = 0.52\% \pm 0.02\%$; 95% confidence level), provided by Elemental Microanalysis, was inserted every 20 unknown samples to ensure the reliability of the analysis.

Total organic carbon (TOC) was measured using a Vario TOC Cube analyzer (Elementar). Prior to organic carbon analysis, the sediments were decarbonated in silver caps by adding HCl (3.7%) in excess to samples placed on a hot plate, until effervescence ceased. A total of 20–30 mg of samples was then analyzed in tin pellets. For that procedure, a B2178 certified material was used ($C = 3.19\% \pm 0.07\%$, 95% confidence level). The carbon:nitrogen ratio (C:N) is widely used to assess the abundance of terrestrial and aquatic components of OM[65].

Total inorganic carbon

The carbonate content was estimated for all samples by calculating the difference between total carbon and organic carbon. Additionally, Bernard calcimetry, a volumetric standardized method conventionally used to estimate the concentration of $CaCO_3$ in comparison with a pure calcite standard[66], was also applied for 7 samples, whenever a notable change was observed in the core. Note that this method consumes about ~1 g of sediment making any high-resolution measurement impossible. In this study, three measurements were performed and averaged. The results showed that both methods provided similar outcomes (see Supplementary Table 1).

Reporting summary

Further information on research design is available in the Nature Portfolio Reporting Summary linked to this article.

Data availability

The data can be found in the supplementary information and are available at E.V. and P.B. Database Lake Ilay sediment core IL226b-num UBGD.300450[DS/OL]. V1. Science Data Bank (2024[2024-07-29]). https://doi.org/10.57760/sciencedb.11496.

Received: 13 December 2023; Accepted: 18 September 2024;

References

1. Geyman, E. C. et al. The origin of carbonate mud and implications for global climate. *Proc. Natl. Acad. Sci. USA* **119**, e2210617119 (2022).
2. Magny, M. & Ruffaldi, P. Younger Dryas and early Holocene lake-level fluctuations in the Jura mountains, France. *Boreas* **24**, 155–172 (1995).
3. Liu, X. et al. A 16000-year pollen record of Qinghai Lake and its paleoclimate and paleoenvironment. *Chin. Sci. Bull.* **47**, 1931–1936 (2002).
4. Trower, E. J., Lamb, M. P. & Fischer, W. W. The origin of carbonate mud. *Geophys. Res. Lett.* **46**, 2696–2703 (2019).
5. Einsele, G., Yan, J. & Hinderer, M. Atmospheric carbon burial in modern lake basins and its significance for the global carbon budget. *Global Planet. Chang.* **30**, 167–195 (2001).
6. Tutolo, B. & Tosca, N. J. Dry, salty, and habitable: the science of alkaline lakes. *Elements* **19**, 10–14 (2023).
7. Lowenstam, H. A. & Epstein, S. On the origin of sedimentary aragonite needles of the Great Bahama Bank. *J. Geol.* **65**, 364–375 (1957).
8. Neumann, A. C. & Land, L. S. Lime mud deposition and calcareous algae in the Bight of Abaco, Bahamas: a budget. *J. Sediment. Petrol.* **45**, 763–786 (1975).
9. Shinn, E., Steinen, R. P., Lidz, B. H. & Swart, P. K. Whitings, a sedimentologic dilemma. *J. Sediment. Petrol.* **59**, 147–161 (1989).
10. Thompson, J. B., Schultze-Lam, S., Beveridge, J. & Des Marais, D. J. Whiting events: biogenic origin due to the photosynthetic activity of cyanobacterial picoplankton. *Limnol. Oceanogr.* **42**, 133–141 (1997).
11. Escoffier, N. et al. Whiting events in a large peri-alpine lake: evidence of a catchment-scale process. *J. Geophys. Res. Biogeosci.* **127**, e2022JG006823 (2022).
12. Dupraz, C. & Visscher, P. T. Microbial lithification in marine stromatolites and hypersaline mats. *Trends Microbiol.* **13**, 429–438 (2005).

13. Stanton, C., Barnes, B. D., Kump, L. R. & Cosmidis, J. A re-examination of the mechanism of whiting events: a new role for diatoms in Fayetteville Green Lake (New York, USA). *Geobiology* **21**, 210–228 (2023).
14. Mathews, R. Genesis of recent lime mud in southern British Honduras. *J. Sediment. Res.* **36**, 428–454 (1966).
15. Glunk, C. et al. Microbially mediated carbonate precipitation in a hypersaline lake, Big Pond (Eleuthera, Bahamas): Microbially mediated carbonate precipitation. *Sedimentology* **58**, 720–736 (2011).
16. Pace, A. et al. Microbial and diagenetic steps leading to the mineralisation of Great Salt Lake microbialites. *Sci. Rep.* **6**, 1–12 (2016).
17. Vennin, E. et al. The lacustrine microbial carbonate factory of the successive Lake Bonneville and Great Salt Lake, Utah, USA. *Sedimentology* **66**, 165–204 (2019).
18. Krumbein, W. E. & Stal, L. J. The geophysiology of marine cyanobacterial mats and biofilms. *Kiel. Meeresforsch. Sonderh.* **8**, 137–145 (1991).
19. Rossi, F. & De Philippis, R. Role of cyanobacterial exopolysaccharides in phototrophic biofilms and in complex microbial mats. *Life* **5**, 1218–1238 (2015).
20. Braissant, O. et al. Exopolymeric substances of sulfate-reducing bacteria: interactions with calcium at alkaline pH and implication for formation of carbonate minerals. *Geobiology* **5**, 401–411 (2007).
21. Monty, C. L. V. The rise and nature of carbonate mud-mounds: an introductory actualistic approach. in *Carbonate Mud-Mounds—Their Origin And Evolution* Vol. 23 (eds Monty, C. L. V., Bosence, D. W. J., Bridges, P. H., & Pratt, B. R.) 11–48 (International Association of Sedimentologists, 1995).
22. Sforna, M. C. et al. Patterns of metal distribution in hypersaline microbialites during early diagenesis: implications for the fossil record. *Geobiology* **15**, 259–279 (2017).
23. Monna, F. et al. Modeling of 137Cs migration in soils using an 80-year soil archive: role of fertilizers and agricultural amendments. *J. Environ. Radioact.* **100**, 9–16 (2009).
24. Evrard, O., Chaboche, P. A., Ramon, R., Foucher, A. & Laceby, J. P. A global review of sediment source fingerprinting research incorporating fallout radiocesium (^{137}Cs). *Geomorphology* **362**, 107103 (2020).
25. Richie, J. C. & McHenry, J. R. Application of radioactive fallout cesium-137 for measuring soil erosion and sediment accumulation rates and patterns: a review. *J. Environ. Qual.* **19**, 215–233 (1990).
26. Lamb, A. L., Wilson, G. P. & Leng, M. J. A review of coastal palaeoclimate and relative sea-level reconstructions using d^{13}C and C/N ratios in organic material. *Earth Sci. Rev.* **75**, 29–57 (2006).
27. Mühlenbruch, M., Grossart, H. P., Eigemann, F. & Voss, M. Mini-eview: phytoplankton-derived polysaccharides in the marine environment and their interactions with heterotrophic bacteria. *Environ. Microbiol.* **20**, 2671–22685 (2008).
28. Dupraz, C., Visscher, P. T., Baumgartner, L. K. & Reid, R. P. Microbe–mineral interactions: Early carbonate precipitation in a hypersaline lake (Eleuthera Island, Bahamas). *Sedimentology* **51**, 745–765 (2004).
29. Decho, A. W., Visscher, P. T. & Reid, R. P. Production and cycling of natural microbial exopolymers (EPS) within a marine stromatolite. *Paleogeogr. Paleoclimatol. Paleoecol.* **219**, 71–86 (2005).
30. Kepkay, P. E. & Andersen, F. O. Aerobic and anaerobic metabolism of a sediment enriched with Spartina alterniflora. *Mar. Col. Prog. Sir.* **21**, 153–161 (1985).
31. Megonigal, J. P., Hines, M. E. & Visscher, P. T. Anaerobic metabolism and production of trace gases. in *Treatise on Geochemistry*, Vol. 8 (eds Holland, H. D. & Turekian, K. K.) 317–424 (Elsevier, 2003).
32. Luo, M. et al. Microbially induced carbonate precipitation in a Middle Triassic microbial mat deposit from southwestern China: new implications for the formational process of micrite. *J. Earth Sci.* **32**, 633–645 (2021).
33. Teske, A. "Marine deep sediment microbial communities" in *The Prokaryotes*, (eds Rosenberg, E., DeLong, E. F., Lory, S., Stackebrandt, E. & Thompson, F.) 123–138 (Springer, 2013).
34. Kallmeyer, J., Grewe, S., Glombitza, C. & Kitte, J. A. Microbial abundance in lacustrine sediments: a case study from Lake Van, Turkey. *Int. J. Earth Sci.* **104**, 1667–1677 (2015).
35. Visscher, P. T., Gritzer, R. F. & Leadbetter, E. R. Low-molecular-weight sulfonates, a major substrate for sulfate reducers in marine microbial mats. *Appl. Environ. Microbiol.* **65**, 3272–3278 (1999).
36. Duteil, T. et al. Preservation of exopolymeric substances in estuarine sediments. *Front. Microbiol.* **13**, 921154 (2022).
37. Braissant, O., Cailleau, G., Dupraz, G. P. & Verrecchia, E. Bacterially induced mineralization of calcium carbonatea in terrestrial environments: the role of exopoly-saccharides and amino acids. *J. Sediment. Res.* **73**, 485–490 (2003).
38. Dupraz, C. et al. Processes of carbonate precipitation in modern microbial mats. *Earth Sci. Rev.* **96**, 141–162 (2009).
39. Wheeler, A. P. & Sikes, C. S. Regulation of carbonate calcification by organic matrix. *Amer. Zool.* **24**, 933–944 (1984).
40. Decho, A. W. & Gutierrez, T. Microbial extracellular polymeric substances (EPSs) in ocean systems. *Front. Microbiol.* **8**, 922 (2017).
41. Underwood, G. J. C. & Paterson, D. M. The importance of extracellular carbohydrate production by marine epipelic diatoms. *Adv. Bot. Res.* **40**, 184–240 (2003).
42. Braissant, O. et al. Characteristics and turnover of exopolymeric substances in a hypersaline microbial mat. *FEMS Microbiol. Ecol.* **69**, 293–307 (2009).
43. Martinho de Brito, M. *The Role of Cyanobacterial Extracellular Polymeric Substances (EPS) in Carbonate Precipitation*. PhD thesis, 196 (Univ. Burgundy, 2023).
44. Spadofora, A., Perri, E., Mckenzie, J. A. & Vasconcelos, C. Microbial biomineralization processes forming modern Ca:Mg carbonate stromatolites. *Sedimentology* **57**, 27–40 (2010).
45. Decho, A. W. Microbial biofilms in intertidal systems: an overview. *Cont. Shelf Res.* **20**, 1257–1273 (2000).
46. Pedley, M. The morphology and function of thrombolytic calcite precipitating biofilms: a universal model derived from freshwater mesocosm experiments. *Sedimentology* **61**, 22–40 (2014).
47. Zhuang, D. X. et al. Calcite precipitation induced by Bacillus cereus MRR2 cultured at different Ca^{2+} concentrations: further insights into biotic and abiotic calcite. *Chem. Geol.* **500**, 64–87 (2018).
48. Verspagen, J. M. H. et al. Rising CO$_2$ levels will intensify phytoplankton blooms in eutrophic and hypertrophic lakes. *PloS ONE* **9**, e104325 (2014).
49. Folk, R. L. Some aspects of recrystallization in ancient limestones: in *Dolomitization and Limestone Diagenesis*, Vol. 13 (eds Pray, L. C. & Murray, R. C.) 14–48 (Society of Economic Paleontologists and Mineralogists, 1965).
50. Kaczmarek, S. E., Fullmer, S. M. & Hasiuk, F. J. A universal classification scheme for the microcrystals that host limestone microporosity. *J. Sediment. Res.* **85**, 1197–1212 (2015).
51. Mercedes-Martín, R., Rogerson, M. R., Brasier, A. T., Reijmer, J. J. G. & Pedley, H. M. Towards a morphology diagram for terrestrial carbonates: evaluating the impact of carbonate supersaturation and alginic acid in calcite precipitate morphology. *Geochim. Cosmochim. Acta* **306**, 340–361 (2021).
52. Folk, R. L. Practical petrographic classification of limestones. *Bull. Am. Assoc. Petrol. Geol.* **43**, 1–38 (1959).
53. Bathurst, R. G. C. Boring algae, micrite envelopes, and lithification of molluscan biosparites. *Geol. J.* **5**, 15–32 (1966).
54. Reid, R. P., Macintyre, I. G. & Post, J. E. Micritized skeletal grains in northern Belize lagoon: a major source of Mg-calcite mud. *J. Sediment. Petrol* **62**, 145–156 (1992).

55. Gran, G. Determination of the equivalence point in potentiometric titrations. Part II. *Analyst* **77**, 661–671 (1952).
56. Parkhurst, D. L. & Wissmeier, L. 'PhreeqcRM: a reaction module for transport simulators based on the geochemical model PHREEQC'. *Adv. Water Resour.* **83**, 176–189 (2015).
57. Parkhurst, D. & Appelo, C. Description of input and examples for PHREEQC version 3—a computer program for speciation, batch-reaction, one-dimensional transport, and inverse geochemical calculations. U.S. Geol. Survey Water Resources Investigations Report. https://pubs.usgs.gov/tm/06/a43/ (2013).
58. Kempe, S. & Kazmierczak, J. The role of alkalinity in the evolution of ocean chemistry, organization of living systems, and biocalcification processes. *Bull. Inst. Océanogr.* **13**, 61–117 (1994).
59. Ramsey, C. B. Bayesian analysis of radiocarbon dates. *Radiocarbon* **51**, 337–360 (2009).
60. Reimer, P. J. et al. The IntCal20 Northern Hemisphere radiocarbon age calibration curve (0–55 cal kBP). *Radiocarbon* **62,** 725–757 (2020).
61. Passow, U. & Alldredge, A. L. A dye-binding assay for the spectrophotometric measurement of transparent exopolymer particles (TEP). *Limnol. Oceanogr.* **40**, 1326–1335 (1995).
62. Dubois, M., Gilles, K. A., Harmilton, J. K., Rebers, P. A. & Smith, F. Colorimetric method for determination of sugars and related substances. *Anal. Chem.* **28**, 350–356 (1956).
63. Visscher, P. T., Quist, P. & Van Gemerden, H. Methylated sulfur compounds in microbial mats: in situ concentrations and metabolism by a colorless sulfur bacterium. *Appl. Environ. Microbiol.* **57**, 1758–1763 (1991).
64. Massa, C. et al. A 2500 year record of natural and anthropogenic soil erosion in South Greenland. *Quat. Sci. Rev.* **32**, 119–130 (2012).
65. Meyers, P. A. & Ishiwatari, R. Lacustrine organic geochemistry: an overview of indicators of organic-matter sources and diagenesis in lake-sediments. *Org. Geochem.* **20**, 867–900 (1993).
66. Lamas, F., Irigaray, C., Oteo, C. & Chacón, J. Selection of the most appropriate method to determine the carbonate content for engineering purposes with particular regard to marls. *Eng. Geol.* **81**, 32–41 (2005).

Acknowledgements

This work is a contribution from the SEDS team in the Biogéosciences Laboratory (uB, Dijon, France) to the project Carbostock-Envergure/OSU THETA and Stock-car/OSU THETA. The authors warmly thank DImaCell Facility Imaging Center (INRAE, UBFC, France) and the PEA²t platform (Christophe Loup, Chrono-environnement, UBFC, UMR CNRS 6249, France), which manages and maintains the analytical equipment used in this study. Sample management and valorization benefited from the Research Infrastructure Récolnat (national network of naturalist collections). We are indebted to the reviewers whose comments greatly improved the manuscript and the associate editor Carolina Ortiz Guerrero. We would particularly like to thank the team of divers who allowed us to collect the core samples for this study (Charlène Develay, Joseph Fahys Renny Hintze, Géraldine Motreuil, Maria Teixeira). We also thank Beta Analytic (Miami, USA) for dating and Geosciences Environment Toulouse laboratory (GET, Toulouse, France) for waters analysis. We thank Le Frasnois town hall for granting permission to take samples.

Author contributions

E.V. supervised the project. E.V. and P.B. designed the study, conducted the analysis, and E.V., P.B., and P.V. wrote the manuscript. E.V., P.B., P.V., and F.M. advised on the approach followed and the interpretation of results. E.V., P.B., P.V., F.M., A.B., S.M., L.M., I.B., and D.R. performed the different analyses and prepared the data. All authors reviewed the manuscript and agreed on the final version.

Competing interests

The authors declare no competing interests.

Additional information

Supplementary information The online version contains supplementary material available at https://doi.org/10.1038/s43247-024-01709-9.

Correspondence and requests for materials should be addressed to E. Vennin.

Peer review information *Communications Earth & Environment* thanks Miroslaw Slowakiewicz and the other, anonymous, reviewer(s) for their contribution to the peer review of this work. Primary Handling Editor: Carolina Ortiz Guerrero. A peer review file is available.